ARTICLES

On-the-Fly, Electric-Field-Driven, Coupled Electron−Nuclear Dynamics

Garth A. Jones,*,† Angela Acocella,‡ and Francesco Zerbetto‡

Department of Biological Sciences, University of Essex, Wivenhoe Park, Colchester, CO4 3SQ, United Kingdom, and Dipartimento di Chimica "G. Ciamician", Università di Bologna, V. F. Selmi 2, 40126, Bologna, Italy

Received: December 12, 2007; Revised Manuscript Received: July 17, 2008

An on-the-fly, electric field driven, coupled electron−nuclear dynamics approach is developed and applied to model the photodissociation of water in the $\tilde{A}(^1B_1)$ excited state. In this method, a quantum propagator evolves the photon-induced electronic dynamics in the ultrafast time scale, and a quasi-classical surface hopping approach describes the nuclear dynamics in the slower time scale. In addition, strong system−field interactions are explicitly included in the electronic propagator. This theoretical development enables us to study rapid photon-induced bond dissociation dynamics and demonstrates the partial breakdown of electronic coherence as well as electronic population trapping in the excited state when the molecular vibrations detune the system with respect to the applied field. The method offers a practical way to use on-the-fly dynamics for modeling light−molecule interactions that lead to interesting photochemical events.

1. Introduction

Radiation−matter interactions are fundamental to nature. Significant is the case of the interaction of light with a molecule that gives rise to electronically excited states, a precursor of chemical events such as charge transfer,[1] energy transfer,[2] and the photodissociation of molecules.[3] When a molecule is exposed to a strong laser field, the parameters of the field can play a significant role in product formation. Altering the wavelength can bring transitions into and out of resonance with the incident light. Other parameters such as light intensity, pulse width, and delay time also play important roles in many circumstances.[4,5] These are especially important in the (sub)-femtosecond regime, where the pulse width is of the order of a molecular vibration. Quantum control experiments seek to optimize the outcome of photochemical reactions by fine tuning the parameters of the applied laser field.[6−10] For example, one may wish to increase the yield of a desired fragment in a photodissociative process while at the same time reducing the production of unwanted fragments. Finding the optimal conditions can be very difficult and often involves using statistical techniques to search "for the elusive pulse among hundreds of thousands of shaped pulses following a number of strategies".[6] Laser pump−probe experiments that study ultrafast processes have also made some very exciting advances over the past several years.[11−13] One particularly interesting recent discovery is that long-lived quantum coherence can occur in natural photosynthetic systems.[14,15] This is thought to play a central role in the efficiency of energy transfer within these important biological systems.

Explicit modeling of matter−field interactions can greatly aid the understanding of these ultrafast photon-induced processes.[16−18] Several approaches employ time-dependent quantum chemical methodologies.[19−21] Generally, these approaches involve perturbing the molecular system with a strong field and following the electron dynamics for several femtoseconds. These techniques allow processes such as electronic population transfer between states, charge migration between atoms, and mutiphoton events to be modeled on the ultrafast time scale. However, an underlying feature of most of these models is that they generally assume a stationary molecular geometry, and therefore coupled electron−nuclear effects, such as nuclear-induced electronic decoherence, cannot be addressed. Trajectory surface hopping approaches involve modeling nonadiabatic processes by explicitly incorporating the molecular vibrations via nuclear trajectories that evolve over excited states, as well as ground-state surfaces.[22−24] These methods are very popular because they are robust and can be applied with high precision using either analytical surfaces or by direct-dynamics. Surface hopping methods have been applied to many important phenomena including molecular collisions,[25] photodissociation,[26] and electron transfer.[27] However, these approaches generally do not include the external field or the resulting electron dynamics, and hence there is a lack of detailed information on the ultrafast time scale.

Several studies have been undertaken which involve combining field-driven electron dynamics and nuclear dynamics, with the aim of modeling photodissociation in molecular systems. For example, Dou et al. have employed a complete active-space self-consistent field approach that has been used to model the photodissociation of cyclobutane,[28] and Bargheer et al. have modeled the photodissociation of F_2 and ClF in an argon matrix using a diatomics-in-molecule Hamiltonian.[29] In other studies, Kong and co-workers model photodissociation using a quasi-diatomic approach, where the nuclear motion is described by a wave packet that evolves over a potential energy surface which is "dressed" to mimic interaction with an external

* Corresponding author. Fax: +44 (0)1206 872592. Tel.: +44 (0)12063149. E-mail: garth@essex.ac.uk.
† University of Essex.
‡ Università di Bologna.

10.1021/jp805360v CCC: $40.75
Published on Web 09/04/2008

field,[30−32] and Kono and co-workers employ a time-dependent field-following approach which evolves nuclear wave packets over MCSCF surfaces.[33,34] These types of approaches generally require the construction of analytical ground- and excited-state potential energy surfaces, the dynamics to occur in restricted regions of phase-space, and/or some other approximation to describe the surfaces, such as the use of effective potential terms in the Hamiltonian.

This paper describes the development of an "on-the-fly", coupled electron−nuclear dynamics approach that models photoinduced processes in molecules and gives insight into them. The approach includes the required self-consistency between the electronic and nuclear degrees of freedom by using a quantum propagator to incorporate strong system−field interactions. This quantum propagator is then interfaced with a direct-dynamics surface hopping methodology to treat nuclear dynamics on different excited-state potential energy surfaces. It therefore explicitly includes both the field-induced electron dynamics through the quantum propagator and the molecular vibrations through the quasi-classical dynamics. We have developed the model with the aim of using it to study the influence that both the external field and molecular vibrations play in evolving the quantum subsystem (i.e., the electron dynamics) and how the dynamics of the quantum subsystem can in turn affect the nuclear dynamics of the molecular geometry.

An important feature of the method is that the energies and energy gradients, which are needed to evolve the quasi-classical dynamics, are calculated on the fly using standard quantum chemical methods, thereby avoiding the need to perform the laborious task of constructing analytical surfaces. In addition, we invoke the time scale separation between the rapid electronic process and slower nuclear dynamics to evolve the electronic and nuclear degrees of freedom using small ($\sim 10^{-4}$ fs) and large ($\sim 10^{-1}$ fs) time-steps, respectively. This makes the approach highly robust. The two-step approach is similar in nature to the other methodologies where the dynamics of the electronic and the nuclear degrees of freedom are evolved on fast and slower time scales, respectively.[35−37]

The major difference between this approach over many other on-the-fly quasi-classical dynamics approaches is that it explicitly includes and intimately couples together the laser field parameters, the electron dynamics, and the molecular vibrations. This makes the approach useful for modeling ultrafast events and processes where the laser field parameters and the nuclear dynamics may play important roles in the outcome of a photophysical process, such as issues related to population transfer and coherence dephasing.

In this work, the photodissociation of water was chosen as a test case for this approach because it is one of the most well-studied photoinduced processes. Further, the photodissociation of water from the $\tilde{A}(^1B_1)$ state occurs rapidly and is not complicated by nonadiabatic coupling to other surfaces away from the asymptotic region. Although the model is not expected to provide much additional insight into this well-studied and fundamentally important process, it allows the coupled electron−nuclear dynamics approach to be fully explored and demonstrates that useful insights can be gained when field-driven electron dynamics is coupled to on-the-fly quasi-classical nuclear dynamics. The model demonstrates population trapping in an excited state and partial breakdown of coherence between electronic states when significant distortions of the molecular geometry, induced by the dissociation process, lead to detuning of the system with respect to the external field.

We hope that this approach may prove useful for modeling ultrafast processes where field parameters, electron dynamics, and nuclear dynamics all play important roles. The methodology is fully outlined in section 2.

2. Computational Details

2.1. On-the-Fly Coupled Electron−Nuclear Dynamics. In this section, the coupled electron−nuclear dynamics approach is described without loss of generality. The electronic degrees of freedom are evolved using a quantum propagator which includes the system−field interaction in the form of an intense oscillating external electric field coupled to the transition dipole moment of the molecule. Quasi-classical dynamics are used to evolve the nuclear degrees of freedom by employing the velocity Verlet integrator.[38] The system−field interaction may give rise to electronic transitions if a resonance exists between the applied electric field and one of the allowed transitions. The Tully criterion is used to determine whether this is to occur.[22] If so, the quasi-classical trajectory will begin evolving on the new surface. The algorithm employs a two-step approach where the dynamics of the electronic and the nuclear degrees of freedom are evolved, in turns, and on fast and slower time scales, respectively.

The electron dynamics is driven, on the fast time scale, by an oscillating external electric field, which may be considered to be a simple classical analogue of a laser field.The electron dynamics algorithm employs the norm-conserving Cayley propagator:[39,40]

$$\Psi(t+\delta t) = \left(1 + \frac{iH\delta t}{2\hbar}\right)^{-1}\left(1 - \frac{iH\delta t}{2\hbar}\right)\Psi(t) \qquad (1)$$

where Ψ is the electronic wave function and H is the total Hamiltonian matrix defined by the sum of the unperturbed Hamiltonian, H_o, and the perturbed part of the Hamiltonian $H'(t)$.

$$H(t) = H_o + H'(t) \qquad (2)$$

The total Hamiltonian takes the *energy* or *state* representation, where the unperturbed Hamiltonian matrix is diagonal. The diagonal elements correspond to the eigenvalues of each of the states (scaled so that the ground state is zero). The perturbed part of the Hamiltonian depends on time and is defined by eq 3.

$$H'(t) = -\vec{\mu}\varepsilon(t)\sin(\omega t) \qquad (3)$$

It introduces the field−matter interaction, where the external field is a classical linearly polarized electric field that is coupled to the molecule via the electronic transition dipole moment, $\vec{\mu}$. Here, $\varepsilon(t)$ is the amplitude of the applied electric field and ω is the frequency of the applied field.

In the current application, the molecule is initially in its electronic ground state and the initial wave function is an eigenfunction of the molecular Hamiltonian, with the coefficient corresponding to the ground state being unity and all of the other coefficients being equal to zero. After the external electric field is "switched on", coupling may occur between the ground state and one or more of the excited states. The molecular wave function will then evolve in time, moving from its original stationary ground-state wave function to a nonstationary state, i.e., a state that is a coherent superposition of the energy eigenstates. If the wavelength of the incident radiation is resonant with an allowed transition, electronic population flows between the states. The wave function coefficients now become complex-valued with the elements remaining orthonormal to one another at all times during the entire trajectory.

The density matrix elements may be calculated at any time, t, using eq 4.

$$\rho_{ij}(t) = c_i^*(t)c_j(t) \tag{4}$$

Here $c_i(t)$ and $c_j(t)$ are the complex-valued wave function coefficients, corresponding to states i and j. The diagonal elements, $\rho_{ii}(t)$, are real-valued and describe the population of each of the states as the electron dynamics trajectory proceeds. The trace of the density matrix is unity throughout the trajectory. The off-diagonal elements, $\rho_{ij}(t)$, $i \neq j$, are generally complex-valued and represent the coherences between two different electronic states.

We now discuss how the molecular vibrations are incorporated into the model by employing a direct quasi-classical dynamics routine. The quasi-classical dynamics is coupled to the electron dynamics intimately through a two-step procedure: For every time-step of the quasi-classical dynamics trajectory, the electron dynamics is evolved for exactly the same period using a time-step that is approximately 3 orders of magnitude smaller. Therefore, before each of the quasi-classical dynamics steps begins, the electron dynamics routine will have been evolved for one cycle using the electronic parameters obtained from the previous quasi-classical dynamics step. Once the electron dynamics has completed its cycle, the Tully criterion is applied to assess whether surface hopping should occur using eq 5:[22,23]

$$P_{i\rightarrow j} = \max\left[\frac{\rho_{ii}(t_1) - \rho_{ii}(t_2)}{\rho_{ii}(t_1)}, 0\right] \tag{5}$$

where P is the probability of hopping out of the ith state and into the jth state. Here ρ_{ii} is the population of the ith state, and the jth state corresponds to the state where the majority of the state population moves into. The probability of surface hopping is compared to a pseudorandom number between 0 and 1. If surface hopping is deemed to occur, according to the pseudo-random number, the quasi-classical trajectory begins to evolve on the other surface from the next point of the trajectory. This procedure introduces the quantum-to-classical interaction to the model, namely, that at any point during the quasi-classical trajectory a significant shift of electron population from one state to another state may take place as a result of the electron dynamics. This will in turn affect the nuclear dynamics by enabling the trajectory to evolve on the new potential energy surface.

The quasi-classical dynamics is evolved using the velocity Verlet integrator.[38] In the current study, the forces are calculated numerically from the Hartree−Fock and CIS wave functions, for the ground and excited-state surfaces, respectively. During the running of a coupled electron−nuclear dynamics trajectory, the parameters required to evolve the electron dynamics, namely, the molecule's transition dipole moment and its state energies, are updated at every point of the quasi-classical dynamics trajectory. This introduces the classical-to-quantum interaction, namely, that the quasi-classical dynamics gives rise to changes in the molecular geometry and that these changes, in turn, affect the electronic properties that are required to evolve the quantum subsystem. *The coupled electron−nuclear dynamics approach therefore introduces a forward−backward self-consistency between the electronic and nuclear degrees of freedom.*

There are a few approximations of the model which will now be explicitly stated. The first is the neglect of multiphoton events and/or ionization of the molecules. A high-intensity external field is required for full population inversion to take place. In the current simulation, an intensity of 0.05 au, or 2.57 V Å^{-1} is used. The requirement of high-intensity fields for full population inversion to occur is a common characteristic in these kinds of single-molecule simulations, and intensities of this magnitude are often used.[19−21] In reality, these intensities would be expected to give rise to multiphoton events and/or ionization of the molecules. However, these processes are not considered in the current application. The only electronic processes that are considered within the context of the current model are transitions between the electronic states of the neutral molecule via direct interaction with the external field. A second approximation is that the polarizability of the molecule is neglected. The application of an oscillating external field could lead to a "dressed" surface when the energy levels would fluctuate in response to the applied field. However, for the current application, the frequency of the external perturbation is much higher than that of the rate of transition, and hence we assume that the surfaces take the averaged form. As a result, when the Hartree−Fock or CIS wave functions are calculated at each point of the quasi-classical trajectory, it is done in the absence of an external field. Finally, in the current application, we do not consider the possibility of thermal transitions introduced via the nonadiabatic coupling vector. This can be justified, within the context of the current application, because the first excited singlet state of water is well separated from the other states away from the asymptotic region of the potential energy surface.

TABLE 1: UCIS/6-31++G(d,p) Parameters

state	energy relative to GS (eV)	transition dipole moment (au)
1 ($^3B_1$)	8.09	0.00
2 ($^1B_1$)	8.73	0.472
3 ($^3A_2$)	10.12	0.00
4 ($^3A_1$)	10.15	0.00
5 ($^1A_2$)	10.42	0.00
6 ($^1A_1$)	10.93	0.00

2.2. Ab Initio Calculations. The trajectory described below, which models the photodissociation of water, employs the 6-31++G(d,p) basis set which includes polarization and diffuses functions both on the oxygen and hydrogen atoms. Because we are dealing with a photodissociation process that involves the breaking of an OH bond, unrestricted wave functions are employed. Both Hartree−Fock and configuration interaction singles (CIS) levels of theory are used in the current study.

The water molecule was optimized at the HF/6-31++G(d,p) level of theory. The optimized geometry of water has a structure of C_{2v} symmetry with OH bond lengths of 0.94 Å, and an HOH bond angle of 107.1°. A subsequent harmonic frequency analysis revealed three real-valued normal vibrational modes corresponding to the in-plane bending mode (ν_1 = 1728.8 cm^{-1}), the symmetric OH stretching mode (ν_2 = 4146.4 cm^{-1}), and the antisymmetric OH stretching mode (ν_3 = 4268.5 cm^{-1}).

A UCIS/6-31++G(d,p) calculation was performed on the HF/6-31++G(d,p) optimized structure. The six lowest states were included in the calculation revealing three singlet states and three triplet states. Table 1 displays the important data from the CIS calculations. The transition dipole moments displayed in column three are those associated with the Cartesian coordinate that passes through the plane of the water molecule. (i.e., in the calculations, the water molecule is constrained to the xz-plane and the dipole moment corresponds to the y-direction).

One can see from Table 1 that the only state with a finite transition dipole moment in the y-direction, for the HF/6-31++G(d,p) optimized C_{2v} structure, is the first excited singlet

state, which lies 8.73 eV above the ground state. This corresponds to the $\tilde{A}(^1B_1)$ state and overestimates the experimental value by ∼1 eV.[3,41]

2.3. Initialization and Running of the Coupled Electron−Nuclear Dynamics Trajectory. The trajectory calculations are performed using "in-house" software that has been written in Fortran 90. The software makes use of linear algebra libraries (LAPACK and BLAS).[42,43] During the running of the coupled electron−nuclear dynamics simulations, Gaussian03 is called automatically to calculate the parameters required at each step in the trajectory.[44] The two main parameters that are used to evolve the electron dynamics are the CIS state energies and the transition dipole moments. The forces corresponding to the surface that the trajectory is evolving are the parameters required for the nuclear dynamics. The forces are calculated using the Hartree−Fock wave function when the trajectory is evolving on the ground-state surface and the CIS wave function when it is on one of the excited-state surfaces.

The quasi-classical trajectory was initialized at the C_{2v} optimized geometry and begins on the ground-state surface. Zero-point energy is applied to each of the vibrational modes. The trajectory therefore starts in its ground-state equilibrium position with all vibrational modes having maximum kinetic energy. The quantum trajectory includes the ground state and all six excited states. The initial wave function is therefore the pure ground-state wave function of the form $\Psi(t = 0) = \{1, 0, 0, 0, 0, 0, 0\}$.

When the trajectory begins, the oscillating electronic field is applied into the plane of the water molecule (i.e., that perpendicular to both of the OH bonds) and is applied continuously throughout the simulation. The phase of the external perturbation is initially zero. The maximum intensity of the external oscillating field is set to 2.57 V Å^{-1}. The frequency of the applied field corresponds to a photon energy of 8.73 eV, which is equal to the difference in energy between the ground state and the first excited singlet state, $\tilde{A}(^1B_1)$.

The time-steps used in this trajectory are $\delta t = 1.0 \times 10^{-4}$ and $\Delta t = 0.1$ fs for the electron and nuclear dynamics steps, respectively.

3. Application

3.1. Background. The photodissociation of water is generally considered one of the most studied and best understood examples of photodissociation. Many studies, both experimental and theoretical in nature, have been done on this process.[3,41,45−49] Although the photodissociation of water can occur via a range of possible mechanisms and wavelengths of light, this study is concerned only with the direct and rapid photodissociation that occurs from the first electronically excited singlet state, $\tilde{A}(^1B_1)$ via interaction with light that is resonant with this transition. The photodissociation of water from $\tilde{A}(^1B_1)$ is considered to be a "prototype of fast and direct bond rupture in an excited electronic state".[41] The transition to the lowest energy excited singlet state, $\tilde{A}(^1B_1)$, is well separated from the higher energy singlet states, which implies that photodissociation occurs with very little interaction from these states. The lack of fine structure in its spectral band indicates that dissociation in $\tilde{A}(^1B_1)$ occurs via a direct mechanism, and it is generally accepted that the lifetime of $H_2O(\tilde{A})$ is within the period of a molecular vibration.[3,36] Schematically, the process is described as

$$H_2O(\tilde{X}, {}^1A_1) + \hbar\omega(\approx 165\,\text{nm}) \rightarrow H_2O(\tilde{A}, {}^1B_1) \rightarrow H(^2S) + OH(^2\Pi) \quad (6)$$

Within the context of a coupled electron−nuclear dynamics methodology, the photodissociation can be thought of as taking place in two steps. Initially, the application of radiation at about 165 nm induces an electronic transition from the electronic ground state, $\tilde{X}(^1A_1)$, to the first excited singlet electronic state $\tilde{A}(^1B_1)$. The excited state is unbound. Once the system becomes electronically excited for a significant period of time, the molecular vibrations will move under the influence of the repulsive forces, and rapid photodissociation will result.

3.2. Electron Dynamics Trajectory. Initially, an electron dynamics trajectory was run using the frozen geometry corresponding to the optimized C_{2v} structure. This allows an analysis of the electron dynamics when they are decoupled from the quasi-classical trajectory. Plane-polarized light was propagated into the molecule, in the direction perpendicular to its plane (i.e., the *y*-direction, see section 2.2). The frequency of the incident light, ω, was set in resonance with the energy gap between the ground state and the first excited singlet electronic state $\tilde{A}(^1B_1)$, ΔE. The maximum intensity was set to 2.57 V Å^{-1}. The state populations are defined by the associated diagonal elements from eq 4. After the electric field is applied at time equals zero, rapid population transfer begins to occur immediately from the ground state, $\tilde{X}(^1A_1)$, which has an initial population of 1.0, to the first excited singlet electronic state $\tilde{A}(^1B_1)$, which has an initial population of 0.0. Because the system has a clamped geometry, the incident radiation remains in resonance with the energy gap, ΔE, throughout the electron dynamics trajectory, and full population inversion occurs at approximately 3.3 fs, where 100% of the state population is now in the $\tilde{A}(^1B_1)$ state. Following this, stimulated emission begins to occur, and the ground state becomes fully populated once again at 6.6 fs. These processes continue, in turn, periodically throughout the trajectory, giving rise to two-state coherent excitation between these two active states. Within the context of semiclassical time-dependent perturbation theory, this can be considered to be an *n-photon* process giving rise to absorption and stimulated emission between the two states. The Rabi frequency for this process is 0.0234 au. The analytical solution for the Rabi angular frequency is given by, $\varpi_{ij} = \vec{\mu}_{ij} \cdot \vec{\varepsilon}_0 / \hbar$, where $\vec{\mu}_{ij}$ is the transition dipole moment between states *i* and *j* and $\vec{\varepsilon}_0$ is the amplitude of the incident field. With the use of this formula, the Rabi frequency is 0.0236 au, which is in good agreement with the frequency of population inversion predicted by the quantum propagator.

3.3. Coupled Electron−Nuclear Dynamics. Now the full coupled electron−nuclear dynamics trajectory is considered where zero-point kinetic energy is assigned to each of the three vibrational modes. The trajectory starts near the C_{2v} stationary point, as described in section 2.3. The wave function is initialized in the ground state, and as above, the external electric field is propagated into the plane of the molecule, with a photon energy of 8.73 eV, and a maximum intensity of 2.57 V Å^{-1}. The external field perturbation is continuous with its phase preserved over the entire trajectory. The trajectory runs for 20 fs, which is more than twice the period of an OH stretching mode. Figure 1 describes the dynamics of some of the important parameters as the trajectory evolves over the 20 fs.

When the field is "switched on" at time zero, it is immediately in resonance with the energy gap, ΔE. For the first two femtoseconds, the state population, Figure 1a, begins to move rapidly from the ground state, $\tilde{X}(^1A_1)$, into the first excited singlet state, $\tilde{A}(^1B_1)$. During this period, the vibrational dynamics induces one of the bond lengths, $d(OH_1)$, to increase (Figure 1c), causing ΔE to decrease (Figure 1b). As this OH bond continues to stretch, ΔE gets smaller, and the system moves

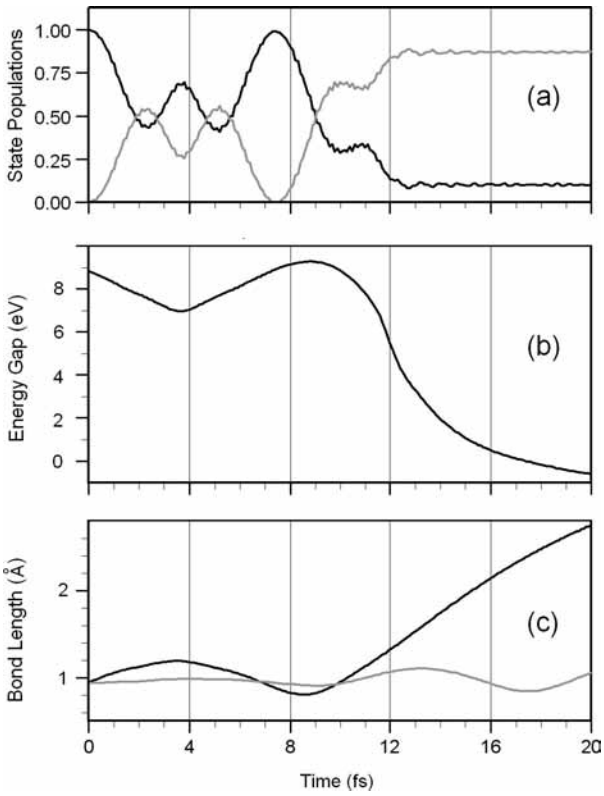

Figure 1. Coupled electron−nuclear dynamics. (a) The state populations for the ground state, $\tilde{X}(^1A_1)$ (black), and the excited state, $\tilde{A}(^1B_1)$ (gray). (b) The energy gap between the ground state and the first excited singlet state, $\tilde{A}(^1B_1)$, in eV. (c) The OH bond lengths, OH_1 (black) and OH_2 (gray), in angstroms.

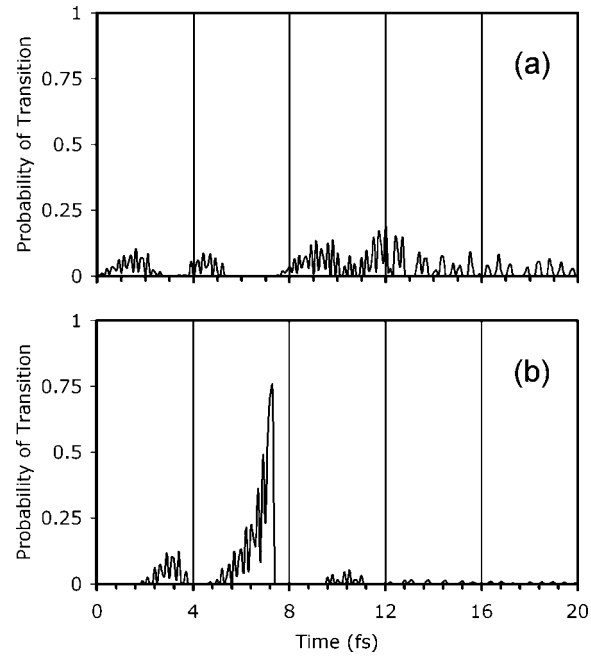

Figure 2. Instantaneous probability of surface hopping according to the Tully criterion, eq 5. (a) Surface hopping from the ground state (lower surface) to the first excited singlet state (upper surface), and (b) the probability of surface hopping from the upper to the lower surface.

out of resonance with the applied field, stopping full population inversion from taking place. State population now begins to flow from the excited state back into the ground state at about the 3 fs mark, and the nuclear trajectory does not enter the excited-state surface. Just before the 4 fs point, the OH bond reaches its maximum length of about 1.2 Å. During the next period (>4 fs), the length of the OH bond decreases, and the trajectory moves back toward the equilibrium geometry. This brings ΔE back into resonance with the applied field, and the state populations flow freely from $\tilde{X}(^1A_1)$ to $\tilde{A}(^1B_1)$ and then back into $\tilde{X}(^1A_1)$, passing a point (~7 fs) where there is nearly 100% population in the ground state.

Figure 2 shows the probability of surface hopping between the ground state, $\tilde{X}(^1A_1)$, and the first excited singlet state, $\tilde{A}(^1B_1)$, based on the Tully criterion, eq 5, where Figure 2a represents the probability of hopping from the ground-state surface to the upper surface and Figure 2b is the probability of hopping from the upper surface back down to the lower surface.

Looking at Figure 2a, one can see that up until the 7 fs mark, there are two short periods where hopping from the ground state to the first excited singlet state has a finite probability. When this is compared to Figure 1a, it can be seen that these periods are centered around the points in the trajectory where the state populations cross (at about 2.0 and 4.5 fs) and the electron population begins to move into the first excited singlet state. The trajectory does in fact hop onto the upper surface at approximately 4.5 fs. However, the trajectory almost immediately hops back down to the ground state before the 7 fs mark, where, one can see from Figure 2b, that the hopping probability for this process is exceptionally high in this region of the trajectory.

During the interval 8−13 fs, Figure 1 shows that the trajectory enters a region of the potential energy surface where ΔE is in resonance with the external field, and a large fraction of the state population moves from the ground state into the first excited singlet state. Again, one can see clearly from Figure 2a that the Tully criterion predicts a high probability of surface hopping to the excited-state surface during this period of the trajectory. The state populations cross at about 9 fs, and at about this point the trajectory hops to the excited-state surface.

The trajectory now having hopped from the bounded $\tilde{X}(^1A_1)$ ground state to the repulsive $\tilde{A}(^1B_1)$ excited state moves along the bond breaking reaction coordinate, and $d(OH_1)$ becomes elongated while simultaneously ΔE becomes smaller. This forces detuning of the system as ΔE moves out of resonance with the applied field. The trajectory is now trapped in the unbounded excited state because stimulated emission can no longer occur. One can see from Figure 2b that there is essentially zero probability of surface hopping from the excited state back into the ground state after the 11 fs mark of the trajectory. Now that the trajectory is trapped on the upper surface, the state populations quickly converge to approximately 0.10 and 0.87 for the ground and first excited singlet states, respectively. Rapid photodissociation then occurs to produce the two products, $H(^2S)$ and $OH(^2\Pi)$.

Figure 3 describes the time dependence of the electronic coherence between the ground state and the first excited state for the first 30 fs of the trajectory. The electronic coherence corresponds to the off-diagonal density matrix element, ρ_{ij}, $i \neq j$, (only the real part is shown), which is associated with the active states, $\tilde{X}(^1A_1)$ and $\tilde{A}(^1B_1)$. Several rigorous theoretical studies have been undertaken on nuclear-induced decoherence, which introduce the nuclear dynamics through Duschinsky rotation[50] and nonadiabatic trajectories.[51,52] In the current presentation we seek only to demonstrate that nuclear-induced decoherence is observed by the model, and hence it is only discussed qualitatively. Note that in the current situation we

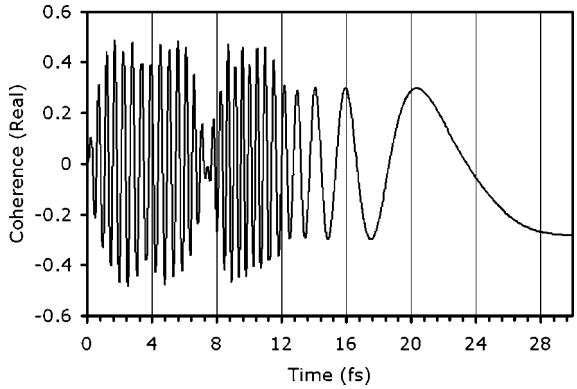

Figure 3. Coherence parameter vs time. This is the (real part of) off-diagonal density matrix element corresponding to the interaction between the ground state, $\tilde{X}(^1A_1)$, and the first excited singlet state, $\tilde{A}(^1B_1)$. Partial nuclear-induced decoherence can be seen after 12 fs, when photodissociation begins to take place.

are dealing with a single gas-phase molecule that has zero-point vibrational energy assigned to each of its normal modes and is exposed to an external field. We did not average over an ensemble of trajectories, nor did we consider the case of system−bath decoherence, where the quantum subsystem is coupled to an external dissipative environment, which is required for condensed phase simulations.[2,53,54]

For the initial part of the trajectory, 0−7 fs, the characteristic oscillations corresponding to a rapid Rabi process can be clearly seen. As expected, the amplitude approaches zero at approximately 7 fs where almost 100% of the state population moves back into the ground state (see Figure 1a). From 7−12 fs, the oscillations associated with coherent electronic population transfer return, as state population once again shifts from the ground state to the first excited singlet state. After the trajectory hops to the excited state, and the photodissociation process begins to take place at about 12 fs, the molecular vibrations drive the molecule out of resonance with the applied field, and partial nuclear-induced decoherence of the quantum subsystem becomes apparent. Two major changes in the dynamics of the coherence parameter can be seen from this point of the trajectory, namely, a reduction in the maximum absolute amplitude and a decay of the frequency of oscillation. The former is related to convergence of the state populations (Figure 1a), with the latter being attributed to the two states evolving toward quasi-degeneracy (Figure 1c).

Although the UCIS/6-31++G(d,p) calculation, performed on the HF/6-31++G(d,p) C_{2v} optimized structure, revealed that the only transition dipole moment coupled to the ground state was the first excited singlet state, $\tilde{A}(^1B_1)$, one can see that the sum of the final state populations is only 0.97. This is because a second excited singlet state becomes very slightly occupied during the running of this trajectory. The state which become slightly populated corresponds to the third excited singlet state, which corresponds to the state $6(^1A_1)$ in Table 1. This occurs because the coupled electron−nuclear dynamics approach updates the electronic parameters at every point of the quasi-classical dynamics trajectory. Consequently, deformations of the molecular geometry that occur during the simulation can give rise to dramatic changes in the magnitude of state energies and transition dipole moments. Therefore, singlet states which are not in resonance, or that are not even coupled to the ground state at the equilibrium geometry, can move into full or partial resonance with the external field as the trajectory evolves away from this region of the potential energy surface. The final state populations (at the 20 fs mark) are 0.10, 0.87, and 0.03 for the ground state, the first, and the third excited singlet states, respectively. All other states are exactly zero, indicating that none of these states become coupled to the ground state during the running of the trajectory.

4. Conclusion

We have described the development of a coupled electron−nuclear dynamics approach that evolves the electronic and nuclear degrees of freedom in a forward−backward self-consistent manner. This is achieved by application of a quantum propagator that incorporates a strong system−field interaction, which is interfaced with a quasi-classical surface hopping methodology. The model was applied to the photodissociation of water from the first excited singlet state, $\tilde{A}(^1B_1)$. Very fast photodissociation of water, of the order of time of a molecular vibration, from the $\tilde{A}(^1B_1)$ state is predicted, in solid agreement with the many previous studies.[3,36]

The model demonstrates population transfer between two states when they are in resonance with an external oscillating field and shows how this resonance condition can breakdown when geometric distortions of the molecular structure force a detuning between the molecular system and the external field, giving rise to population trapping, and which results in rapid photodissociation. Once photodissociation begins to occurs, and electronic population becomes trapped in the excited state, a decrease in the amplitude and frequency of the corresponding off-diagonal density matrix element is seen, indicating partial nuclear-induced decoherence of the quantum subsystem. The electronic parameters are updated at every point in the coupled electron−nuclear dynamics trajectory, and hence states which are not coupled to the ground state at the equilibrium position may become coupled in other regions of the potential energy surface.

The on-the-fly approach for modeling coupled electron−nuclear dynamics appears to offer useful physical and chemical insights into photoinduced processes occurring in molecules and gives a detailed description of the electron dynamics on the ultrafast time scale. Because the technique uses a simple quantum propagator and obtains the required electronic parameters through standard quantum chemical packages, it is robust and can be applied readily to other molecular systems.

Acknowledgment. G.A.J. gratefully acknowledges the EPSRC for the award of a "Life-Sciences Interface" Fellowship (EP/C532082). We thank Dr. Yuan-Chung Cheng (U.C. Berkeley) for many helpful comments and discussions.

Note Added after ASAP Publication. The Abstract and first paragraph of the Introduction section were revised due to a production error. This article originally posted September 4, 2008. The corrected version posted September 12, 2008.

Supporting Information Available: The initial geometries and velocities, the raw data of the stationary point and CIS calculations, plot of the two-state coherent population transfer versus time, described in section 3.2. This material is available free of charge via the Internet at http://pubs.acs.org.

References and Notes

(1) Balzani,V., Ed. *Electron Transfer in Chemistry*; Wiley-VCH: Weinheim, Germany, 2001.

(2) May, V.; Kühn, O. *Charge and Energy Transfer Dynamics in Molecular Systems*; Wiley-VCH: Weinheim, Germany, 2004.

(3) Schinke, R. *Photodissociation Dynamics*; Cambridge University Press: Cambridge, 1993.
(4) Giusti-Suzor, A.; Mies, F. H.; Dimauro, L. F.; Charron, E.; Yang, B. *J. Phys. B: At. Mol. Opt. Phys.* **1995**, *28*, 309.
(5) Machholm, M.; Suzor-Weiner, A. *J. Chem. Phys.* **1996**, *105*, 971.
(6) Lozovoy, V. V.; Zhu, X.; Gunaratne, T. C.; Harris, D. A.; Shane, J. C.; Dantus, M. *J. Phys. Chem. A* **2008**, *112*, 3789.
(7) Nuernberger, P.; Vogt, G.; Brixner, T.; Gerber, G. *Phys. Chem. Chem. Phys.* **2007**, *9*, 2470.
(8) Wollenhaupt, M.; Engel, V.; Baumert, T. *Annu. Rev. Phys. Chem.* **2005**, *56*, 25.
(9) Lozovoy, V. V.; Dantus, M. *ChemPhysChem* **2005**, *6*, 1970.
(10) Klamroth, T. *J. Chem. Phys.* **2006**, *124*, 144310.
(11) Zewail, A. H. *J. Phys. Chem. A* **2000**, *104*, 5660.
(12) Baltuska, A.; Udem, T.; Uiberacker, M.; Hentschel, M.; Goulielmakis, E.; Gohle, C.; Holzwarth, R.; Yakoviev, V. S.; Scrinzi, A.; Hansch, T. W.; Krausz, F. *Nature (London)* **2003**, *421*, 611.
(13) Kienberger, R.; Goulielmakis, E.; Uiberacker, M.; Baltuska, A.; Yakovlev, V.; Bammer, F.; Scrinzi, A.; Westerwalbesloh, T.; Kleineberg, U.; Heinzmann, U.; Drescher, M.; Krausz, F. *Nature (London)* **2004**, *427*, 817.
(14) Engel, G. S.; Calhoun, T. R.; Read, E. L.; Ahn, T.-K.; Mancal, T.; Cheng, Y.-C.; Blankenship, R. E.; Fleming, G. R. *Nature (London)* **2007**, *446*, 782.
(15) Lee, H.; Cheng, Y.-C.; Fleming, G. R. *Science* **2007**, *316*, 1462.
(16) Cheng, Y.-C.; Fleming, G. R. *J. Phys. Chem. A* **2008**, *112*, 4254.
(17) Kilin, D. S.; Prezhdo, O. V.; Schreiber, M. *J. Phys. Chem. A* **2007**, *111*, 10212.
(18) Ashkenazi, G.; Kosloff, R.; Ratner, M. A. *J. Am. Chem. Soc.* **1999**, *121*, 3386.
(19) Schlegel, H. B.; Smith, S. M.; Li, X. S. *J. Chem. Phys.* **2007**, *126*, 244110.
(20) Li, X. S.; Smith, S. M.; Markevitch, A. N.; Romanov, D. A.; Levis, R. J.; Schlegel, H. B. *Phys. Chem. Chem. Phys.* **2005**, *7*, 233.
(21) Remacle, F.; Nest, M.; Levine, R. D. *Phys. Rev. Lett.* **2007**, *99*, 183902.
(22) Tully, J. C. *J. Chem. Phys.* **1990**, *93*, 1061.
(23) Hack, M. D.; Truhlar, D. G. *J. Phys. Chem. A* **2000**, *104*, 7917.
(24) Jasper, A. W.; Nangia, S.; Zhu, C. Y.; Truhlar, D. G. *Acc. Chem. Res.* **2006**, *39*, 101.
(25) Maiti, B.; Schatz, G. C.; Lendvay, G. *J. Phys. Chem. A* **2004**, *108*, 8772.
(26) Paterson, M. J.; Hunt, P. A.; Robb, M. A.; Takahashi, O. *J. Phys. Chem. A* **2002**, *106*, 10494.
(27) Jones, G. A.; Paddon-Row, M. N.; Carpenter, B. K.; Piotrowiak, P. *J. Phys. Chem. A* **2002**, *106*, 5011.
(28) Dou, Y. S.; Lei, Y. B.; Li, A. Y.; Wen, Z. Y.; Torralva, B. R.; Lo, G. V.; Allen, R. E. *J. Phys. Chem. A* **2007**, *111*, 1133.
(29) Bargheer, M.; Cohen, A.; Gerber, R. B.; Guhr, M.; Korolkov, M. V.; Manz, J.; Niv, M. Y.; Schroder, M.; Schwentner, N. *J. Phys. Chem. A* **2007**, *111*, 9573.
(30) Tang, X. P.; Wang, S. F.; Elshakre, M. E.; Gao, L. R.; Wang, Y. L.; Wang, H. F.; Kong, F. A. *J. Phys. Chem. A* **2003**, *107*, 13.
(31) Wang, S. F.; Tang, X. P.; Gao, L. R.; Elshakre, M. E.; Kong, F. N. *J. Phys. Chem. A* **2003**, *107*, 6123.
(32) Elshakre, M. E.; Gao, L. R.; Tang, X. P.; Wang, S. F.; Shu, Y. F.; Kong, F. N. *J. Chem. Phys.* **2003**, *119*, 5397.
(33) Kono, H.; Koseki, S.; Shiota, M.; Fujimura, Y. *J. Phys. Chem. A* **2001**, *105*, 5627.
(34) Sato, Y.; Kono, H.; Koseki, S.; Fujimura, Y. *J. Am. Chem. Soc.* **2003**, *125*, 8019.
(35) Micha, D. A. *Advances In Quantum Chemistry*; Academic Press: New York, 1999; Vol. 35, p 317.
(36) Li, X. S.; Tully, J. C.; Schlegel, H. B.; Frisch, M. J. *J. Chem. Phys.* **2005**, *123*, 084106.
(37) Worth, G. A.; Hunt, P.; Robb, M. A. *J. Phys. Chem. A* **2003**, *107*, 621.
(38) Verlet, L. *Phys. Rev.* **1967**, *159*, 98.
(39) Graves, J. S.; Allen, R. E. *Phys. Rev. B* **1998**, *58*, 13627.
(40) Acocella, A.; Jones, G. A.; Zerbetto, F. *J. Phys. Chem. A* **2006**, *110*, 5164.
(41) Engel, V.; Staemmler, V.; Vander Wal, R. L.; Crim, F. F.; Sension, R. J.; Hudson, B.; Andresen, P.; Hennig, S.; Weide, K.; Schinke, R. *J. Phys. Chem.* **1992**, *96*, 3201.
(42) Anderson, E.; Bai, Z.; Bischof, C.; Blackford, S.; Demmel, J.; Dongarra, J.; Du Croz, J.; Greenbaum, A.; Hammarling, S.; McKenney, A.; Sorensen, D. *LAPACK Users' Guide*; Society for Industrial and Applied Mathematics: Philadelphia, PA, 1999.
(43) Blackford, L. S.; Demmel, J.; Dongarra, J.; Duff, I.; Hammarling, S.; Henry, G.; Heroux, M.; Kaufman, L.; Lumsdaine, A.; Petitet, A.; Pozo, R.; Remington, K.; Whaley, R. C. *ACM Trans. Math. Software* **2002**, *28*, 135.
(44) Frisch, M. J.; Trucks, G. W.; Schlegel, H. B.; Scuseria, G. E.; Robb, M. A.; Cheeseman, J. R.; Montgomery, J. A., Jr.; Vreven, T.; Kudin, K. N.; Burant, J. C.; Millam, J. M.; Iyengar, S. S.; Tomasi, J. J.; Barone, V.; Mennucci, B.; Cossi, M.; Scalmani, G.; Rega, N.; Petersson, G. A.; Nakatsuji, H.; Hada, M.; Ehara, M.; Toyota, K.; Fukuda, R.; Hasegawa, J.; Ishida, M.; Nakajima, T.; Honda, Y.; Kitao, O.; Nakai, H.; Klene, M.; Li, X.; Knox, J. E.; Hratchian, H. P.; Cross, J. B.; Adamo, C.; Jaramillo, J.; Gomperts, R.; Stratmann, R. E.; Yazyev, O.; Austin, A. J.; Cammi, R.; Pomelli, C.; Ochterski, J. W.; Ayala, P. Y.; Morokuma, K.; Voth, A.; Salvador, P.; Dannenberg, J. J.; Zakrzewski, V. G.; Dapprich, S.; Daniels, A. D.; Strain, M. C.; Farkas, O.; Malick, D. K.; Rabuck, A. D.; Raghavachari, K.; Foresman, J. B.; Ortiz, J. V.; Cui, Q.; Baboul, A. G.; Clifford, S.; Cioslowski, J.; Stefanov, B. B.; Liu, G.; Liashenko, A.; Piskorz, P.; Komaromi, I.; Martin, R. L.; Fox, D. J.; Keith, T.; Al-Laham, M. A.; Peng, C. Y.; Nanayakkara, A.; Challacombe, M.; Gill, P. M. W.; Johnson, B.; Chen, W.; Wong, M. W.; Gonzalez, C.; Pople, J. A. *Gaussian 03*, revision C.02; Gaussian, Inc.: Wallingford, CT, 2004.
(45) van Harrevelt, R.; van Hemert, M. C. *J. Chem. Phys.* **2000**, *112*, 5777.
(46) van Harrevelt, R.; van Hemert, M. C. *J. Chem. Phys.* **2000**, *112*, 5787.
(47) Fillion, J. H.; van Harrevelt, R.; Ruiz, J.; Castillejo, M.; Zanganeh, A. H.; Lemaire, J. L.; van Hemert, M. C.; Rostas, F. *J. Phys. Chem. A* **2001**, *105*, 11414.
(48) Chen, F.; McCoy, A. B. *J. Phys. Chem. A* **2003**, *107*, 7220.
(49) Kumar, A.; Kołaski, M.; Lee, H. M.; Kim, K. S. *J. Phys. Chem. A* **2008**, *112*, 5502.
(50) Hwang, H.; Rossky, P. J. *J. Phys. Chem. B* **2004**, *108*, 6723.
(51) Bedard-Hearn, M. J.; Larsen, R. E.; Schwartz, B. J. *J. Chem. Phys.* **2005**, *123*, 234106.
(52) Jasper, A. W.; Truhlar, D. G. *J. Chem. Phys.* **2005**, *123*, 064103.
(53) Cheng, Y.-C.; Engel, G. S.; Fleming, G. R. *Chem. Phys.* **2007**, *341*, 285.
(54) Breuer, H.-B.; Petruccione, F. *The Theory of Open Quantum Systems*; Clarendon Press: Oxford, 2006.

JP805360V